

Intermediately coupled type-II superconductivity in a La-based kagome metal La_3Al

Yingpeng Yu(于英鹏), Zhaolong Liu(刘兆龙), Zhaoxu Chen(陈昭旭), Qi Li(李琦), Yulong Wang(王玉龙), Xuhui Wang(王旭辉), Chunsheng Gong(龚春生), Zhaotong Zhuang(庄照通), Bin-Bin Ruan(阮彬彬), Huifen Ren(任会芬), Peijie Sun(孙培杰), Jian-Gang Guo(郭建刚), and Shifeng Jin(金士锋)

Citation: Chin. Phys. B, 2025, 34 (**1**): 017401. DOI: 10.1088/1674-1056/ad8f9f

What follows is a list of articles you may be interested in

Half-integer Shapiro steps in MgB_2 focused He ion beam Josephson junctions

Dali Yin(殷大利), Xinwei Cai(蔡欣炜), Tiequan Xu(徐铁权), Ruining Sun(孙瑞宁), Ying Han(韩颖), Yan Zhang(张焱), Yue Wang(王越), and Zizhao Gan(甘子钊)

Chin. Phys. B, 2024, 33 (**8**): 087404. DOI: 10.1088/1674-1056/ad4d62

Two-fold symmetry of the in-plane resistance in kagome superconductor $Cs(V_{1-x}Ta_x)_3Sb_5$ with enhanced superconductivity

Zhen Zhao(赵振), Ruwen Wang(王汝文), Yuhang Zhang(张宇航), Ke Zhu(祝轲), Weiqi Yu(余维琪), Yechao Han(韩烨超), Jiali Liu(刘家利), Guojing Hu(胡国静), Hui Guo(郭辉), Xiao Lin(林晓), Xiaoli Dong(董晓莉), Hui Chen(陈辉), Haitao Yang(杨海涛), and Hong-Jun Gao(高鸿钧)

Chin. Phys. B, 2024, 33 (**7**): 077406. DOI: 10.1088/1674-1056/ad4ffa

Observation of parabolic electron bands on superconductor $LaRu_2As_2$

Xingtai Zhou(周兴泰), Geng Li(李更), Lulu Pan(潘禄禄), Zichao Chen(陈子超), Meng Li(李萌), Yanhao Shi(时延昊), Haitao Yang(杨海涛), and Hong-Jun Gao(高鸿钧)

Chin. Phys. B, 2024, 33 (**7**): 077401. DOI: 10.1088/1674-1056/ad4d63

Superconductivity in kagome metal $ThRu_3Si_2$

Yi Liu(刘艺), Jing Li(厉静), Wu-Zhang Yang(杨武璋), Jia-Yi Lu(卢佳依), Bo-Ya Cao(曹博雅), Hua-Xun Li(李华旬), Wan-Li Chai(柴万力), Si-Qi Wu(武思祺), Bai-Zhuo Li(李佰卓), Yun-Lei Sun(孙云蕾), Wen-He Jiao(焦文鹤), Cao Wang(王操), Xiao-Feng Xu(许晓峰), Zhi Ren(任之), and Guang-Han Cao(曹光旱)

Chin. Phys. B, 2024, 33 (**5**): 057401. DOI: 10.1088/1674-1056/ad1c5e

Robust T_c in element molybdenum up to 160 GPa

Xinyue Wu(吴新月), Shumin Guo(郭淑敏), Jianning Guo(郭鉴宁), Su Chen(陈诉), Yulong Wang(王煜龙), Kexin Zhang(张可欣), Chengcheng Zhu(朱程程), Chenchen Liu(刘晨晨), Xiaoli Huang(黄晓丽), Defang Duan(段德芳), and Tian Cui(崔田)

Chin. Phys. B, 2024, 33 (**4**): 047406. DOI: 10.1088/1674-1056/ad2a78

Intermediately coupled type-II superconductivity in a La-based kagome metal La_3Al

Yingpeng Yu(于英鹏)[1,2], Zhaolong Liu(刘兆龙)[1,3], Zhaoxu Chen(陈昭旭)[1,4], Qi Li(李琦)[1,3], Yulong Wang(王玉龙)[1,4], Xuhui Wang(王旭辉)[1,2], Chunsheng Gong(龚春生)[5], Zhaotong Zhuang(庄照通)[1,2], Bin-Bin Ruan(阮彬彬)[1], Huifen Ren(任会芬)[1,2], Peijie Sun(孙培杰)[1], Jian-Gang Guo(郭建刚)[1,6], and Shifeng Jin(金士锋)[1,†]

[1] *Beijing National Laboratory for Condensed Matter Physics and Institute of Physics, Chinese Academy of Sciences, Beijing* 100190, *China*
[2] *University of Chinese Academy of Sciences, Beijing* 100049, *China*
[3] *College of Materials Science and Opto-Electronic Technology, University of Chinese Academy of Sciences, Beijing* 101408, *China*
[4] *School of Physical Sciences, University of Chinese Academy of Sciences, Beijing* 100049, *China*
[5] *Beijing Lattice Semiconductor Co., Ltd., Beijing* 101300, *China*
[6] *Songshan Lake Materials Laboratory, Dongguan* 523808, *China*

(Received 14 August 2024; revised manuscript received 5 November 2024; accepted manuscript online 7 November 2024)

We present a comprehensive investigation into the superconducting properties of La_3Al, a La-based metal with a kagome structure. La_3Al crystallizes in a Ni_3Sn-type crystal structure (space group $P6_3/mmc$), where the La atoms form a kagome lattice. Resistivity measurements reveal superconducting transition with $T_c^{onset} = 6.37$ K and $T_c^{zero} = 6.18$ K. In magnetic susceptibility measurements, the superconducting transition is observed at 6.16 K. The lower and upper critical fields are determined to be 22.17 mT and 6.69 T, respectively. Heat capacity measurements confirm the bulk superconductivity, showing a normalized specific heat change of $\Delta C_e/(\gamma T_c) = 2.16$ and an electron–phonon coupling strength of $\lambda_{ep} = 0.92$. DFT calculations reveal the intricate band structure of La_3Al. The notable specific heat jump, coupled with the electron–phonon coupling strength λ_{ep}, indicates that La_3Al exhibits characteristics of an intermediately coupled type-II superconductor.

Keywords: La_3Al, superconductivity, kagome lattice

PACS: 74.70.Ad, 74.25.F–, 74.25.Jb, 74.25.Ha

DOI: 10.1088/1674-1056/ad8f9f **CSTR:** 32038.14.CPB.ad8f9f

1. Introduction

Compounds with kagome lattice structures, characterized by a two-dimensional network of corner-sharing triangles, have recently attracted significant attention due to their unique electronic structures and magnetic frustration.[1,2] This has provided an exciting platform for exploring various quantum physics phenomena such as quantum spin liquids,[3–6] nontrivial band topology[7–9] and superconductivity.[10–16] In recent years, a newly identified family of materials featuring a V-based kagome lattice, AV_3Sb_5 (where A represents K, Rb, and Cs),[11] has demonstrated superconductivity with transition temperatures (T_c) ranging from 0.93 K to 2.5 K.[12–14] These materials have exhibited several intriguing phenomena, including the anomalous Hall effect,[15] unconventional chiral CDW order,[16–18] pair density wave (PDW),[19] topologically nontrivial band structures,[12,20] pressure-induced two-dome superconductivity[21,22] and improvement in superconductivity by hole doping.[23] Given the diverse properties observed in the AV_3Sb_5 system, further research on other material systems with kagome structures holds significant importance.[24–26]

The RE_3Al system (RE = La, Ce, Pr and Nd) with a Ni_3Sn structure has also garnered attention due to its kagome lattice structure formed by RE atoms and its magnetism, superconductivity and topological properties.[27–36] Among these, the heavy fermion compound Ce_3Al exhibits antiferromagnetic order, the Kondo effect and abnormal structural transitions,[31,32] with theoretical predictions of novel topological properties.[33] Pr_3Al displays ferromagnetic and antiferromagnetic phases, with pressure regulation leading to the emergence of new ferromagnetic phases.[37] Nd_3Al exhibits a long-range ferromagnetic state, along with abnormal Hall coefficients and topological Hall effects in this state.[31,35,36] In contrast, research on La_3Al, the sole superconducting material in this series with a respective high T_c around 6 K, remains limited. The kagome lattice structure of La_3Al offers a unique opportunity to investigate the interaction between kagome lattice geometry and superconductivity.

The superconductivity in La_3Al was reported in 1967, where the T_c is reported to increase from 5.57 K at ambient pressure to 6.37 K at 8 kbars.[38] Subsequent studies have found that magnetic element doping on La sites will inhibit the superconductivity in La_3Al.[39–42] Notably, in investigating the $(Ce_{1-x}La_x)_3Al$ solid solutions, an anomaly in the resistivity curve is reported in La_3Al around 52 K.[30] X-ray

†Corresponding author. E-mail: shifengjin@iphy.ac.cn

© 2025 Chinese Physical Society and IOP Publishing Ltd. All rights, including for text and data mining, AI training, and similar technologies, are reserved.

diffraction (XRD) measurements have revealed no evidence of structural phase transition at low temperature, suggesting the changes in the structure were too subtle to be resolved by diffraction experiments. To date, the origin of the kink in the resistivity curve of La_3Al remains unclear and has received limited attention. In addition, the detailed superconductivity properties of La_3Al have not been revealed so far.

In this paper, we synthesized La_3Al samples with $T_c^{zero} = 6.37$ K, and performed a detailed analysis of the superconducting properties of this compound. The upper and lower critical fields, coherence length, magnetic penetration length and electron–phonon coupling constant of La_3Al are reported. Additional Hall effect measurement of La_3Al reveals a varying trend in the R_H curve around 40 K, similar to other typical CDW materials and suggests that the transition may have an electronic origin. Through an examination of magnetism, resistivity and specific heat, we confirm that La_3Al behaves as an intermediately coupled type-II superconductor.

2. Experiment and methods

We synthesized polycrystalline La_3Al samples using an arc melting method. Lanthanum (99.9% purity) and aluminum (99.9% purity) powder were thoroughly mixed in a 3:1 molar ratio and pressed into pellets. These pellets underwent at least six arc-melting cycles in a high-purity argon atmosphere with periodic turnovers, resulting in weight loss of less than 1%. The final products exhibited metallic luster and were prone to gradual degradation upon exposure to air over a period of a few days.

Powder x-ray diffraction (pXRD) data were collected at room temperature using a PANalytical x-ray diffractometer with Cu-$K\alpha$ radiation, and crystal structure was generated using VESTA.[43] The elemental compositions were checked by Oxford X-Max energy dispersive x-ray (EDX) spectroscopy analysis using a Hitachi S-4800 scanning electron microscope. Measurements of transport, magnetic and thermodynamic properties were conducted using a physical property measurement system (PPMS, Quantum Design) and a vibrating sample magnetometer (VSM, Quantum Design). The sample was cut into rectangular shapes using a wire cutting machine. Hall electrical resistivity measurements were conducted using a five-probe method, with the current flowing in the *ab* plane of the polycrystalline sample. To eliminate the contribution of longitudinal resistivity arising from misalignment of the voltage probes, the Hall resistivity was determined by calculating the average difference in the transverse resistivity recorded under positive and negative magnetic fields, expressed as $\rho_{yx}(\mu_0 H) = [\rho_{yx}(+\mu_0 H) - \rho_{yx}(-\mu_0 H)]/2$.

First-principles calculations were carried out using density functional theory (DFT) implemented in the Vienna *ab initio* simulation package (VASP).[44] We adopted the generalized gradient approximation (GGA) in the form of the Perdew–Burke–Ernzerhof (PBE)[45] for the exchange–correlation potentials. The projector-augmented-wave (PAW)[46] pseudopotentials were used with a plane wave energy of 600 eV. The $5d^1 6s^2$ electronic configuration of La and $3s^2 3p^1$ electronic configuration of Al were treated as valence electrons, respectively. A Monkhorst–Pack Brillouin zone sampling grid[47] with a resolution of $0.02 \times 2\pi$ Å^{-1} was applied. Atomic positions and lattice parameters were relaxed until all the forces on the ions were less than 10^{-2} eV/Å. In calculating the electronic structure, the spin–orbit coupling (SOC) effect was included.

3. Results

3.1. Structural characterization

The powder pattern confirms the successful formation of the intended La_3Al phase with indexed lattice parameters $a = b = 7.1930$ Å, $c = 5.5007$ Å and crystallization in the hexagonal Ni_3Sn structure (space group $P6_3/mmc$), as shown in Fig. 1(a). We performed energy spectrum scanning on the La_3Al polycrystalline sample, which was polished into a clean and tidy flat surface. The atomic molar ratio of La element and Al element was 74.35%:25.66%, which was close to the ideal ratio of 75%:25%, as shown in the inset of Fig. 1(a). Note that during the measuring, we select multiple areas for surface mapping, and take the average value. Figures 1(b) and 1(c) depict the schematic crystal structure of La_3Al, where the La atoms form a kagome structure, with Al atoms located at the center of the kagome lattice.

3.2. Superconducting properties

Figure 2(a) depicts the temperature-dependent resistivity $\rho(T)$ of La_3Al measured from 1.8 K to 300 K. The gradual decrease in resistivity as temperature decreases indicates a metallic behavior, with the relatively modest residual resistivity ratio (RRR) of 5.97 (calculated as 38.55/6.45) primarily attributed to grain boundary effects. A significant decrease in resistivity is evident at 6.37 K (see inset in Fig. 2(a)), marking the onset of a superconducting transition. At 6.18 K, the resistivity drops to zero, indicating the T_c^{zero} of a superconducting transition. Furthermore, the $4\pi\chi$ curves of magnetic susceptibility in Fig. 2(b) display diamagnetic transitions at 1 mT, with the determined T_c at 6.16 K, nearly consistent with values derived from the $\rho(T)$ curve and heat capacity measurements presented below. A complete Meissner state is attained at approximately 5.0 K. Examination of the zero-field-cooling (ZFC) curve at 2.0 K suggests a superconducting volume fraction (SVF) of roughly 164%, indicating bulk superconductivity. The notable SVF observed in field-cooling (FC) mode implies weak flux pinning effects.

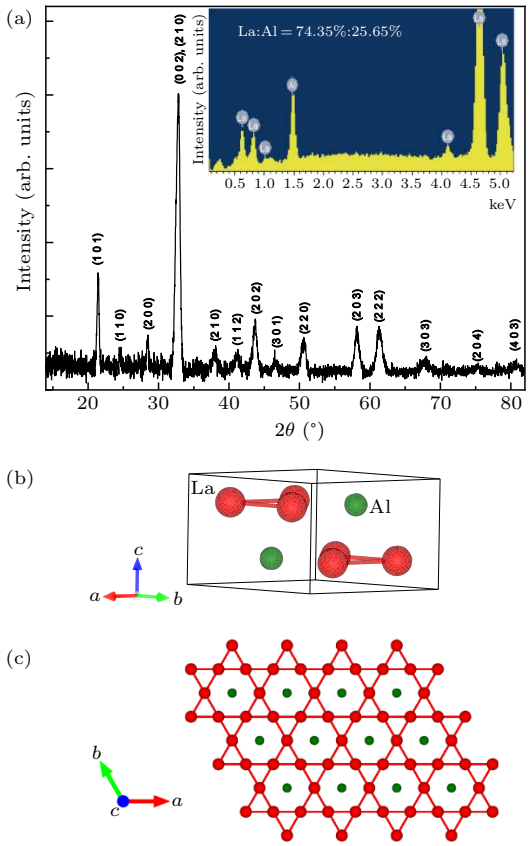


Fig. 1. (a) The pXRD pattern of La_3Al. Inset is energy-dispersive x-ray spectra of La_3Al. (b) Conventional unit cell of La_3Al. (c) La atoms form a kagome lattice with Al atoms in the center of the kagome lattice.

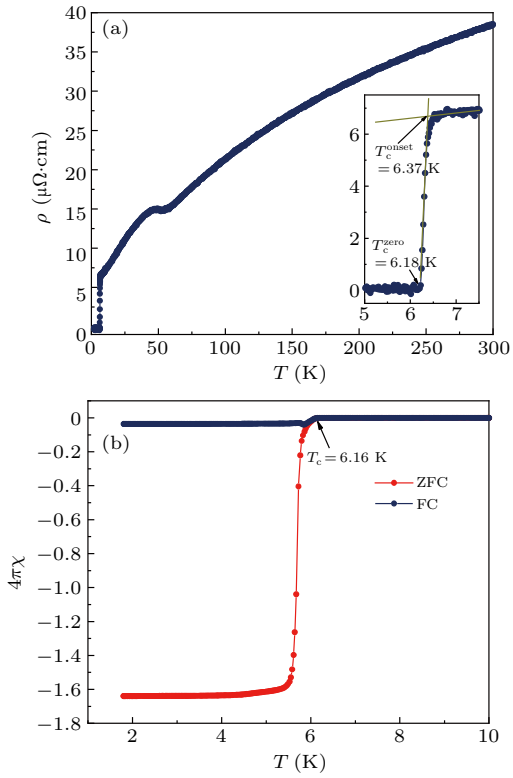


Fig. 2. (a) Temperature dependence of electrical resistivity $\rho(T)$ at zero field for La_3Al. Inset: enlarged view of $\rho(T)$ curves between 5.0 K and 7.5 K. (b) Temperature dependence of magnetic susceptibility $4\pi\chi$ for La_3Al measured at 1 mT with zero-field-cooling (ZFC) and field-cooling (FC) modes.

Notably, from the resistivity versus temperature curve, an obvious anomaly was observed between 40 K and 50 K, which is similar to the findings of Chen *et al.*[30] Considering previous x-ray diffraction experiments near this temperature revealed no evidence of structure phase transition, we measured the Hall resistivity of the sample near the temperature of this anomaly. Figures 3(a) and 3(b) show the field dependence of Hall resistivity $\rho_{xy}(T, \mu_0 H)$ at several typical temperatures, which exhibits a linear behavior against the magnetic field at all temperature ranges from 20 K to 60 K, indicating that the carrier density is dominated by one band. The Hall resistivity curves can be well fitted with linear fits, and thus the temperature-dependent Hall coefficient R_H can be obtained. In Fig. 3(c), the negative Hall coefficient R_H suggests that the electron-type carriers are dominant. As the temperature increases, R_H increases and reaches its maximum at 40 K, which is slightly below the temperature (47 K) of the inflection point in the resistivity at zero magnetic field. When the temperature continues to rise, R_H begins to decrease, so that R_H has a maximum value at 40 K. As the temperature increases from 20 K, the mobility of La_3Al gradually increases. When the temperature is 40 K, the mobility reaches the maximum value. As the temperature continues to rise, the mobility gradually decreases. Notably, the R_H and mobility of La_3Al reached its maximum around the resistivity anomaly, a finding similar to the cases of KV_3Sb_5, RbV_3Sb_5 and CsV_3Sb_5,[48–50] as well as other superconductors with CDW orders, such as $TaSe_2$, TaS_2.[51] and (2H-, 4H-)$NbSe_2$.[52]

Furthermore, we investigated the thermoelectric properties of La_3Al. As shown in Fig. 4(a), we present the temperature dependence of the Seebeck coefficient, S–T, for La_3Al over the range of 2–300 K. Near room temperature, S is negative. As the temperature decreases, S increases rapidly, transitioning from negative to positive around 267 K. Upon further cooling, S initially continues to increase before decreasing again, exhibiting an anomaly near 50 K where S begins to decline noticeably. This behavior is clearly observable in the enlarged S–T curve from 10 K to 100 K in Fig. 4(b), indicating a transition occurred in La_3Al at this temperature. As the temperature decreases further and approaches the superconducting critical temperature, S undergoes another rapid decline, ultimately returning to negative values. In addition, as depicted in Fig. 4(c), we plot the dS/dT–T curve from 2 K to 300 K, which visually highlights the occurrence of two distinct transitions. For comparison, we include the S–T curves of the prototypical charge density wave (CDW) superconductors 2H-$NbSe_2$ and 4H-$NbSe_2$. The S–T curve of La_3Al exhibits similarities to those of these CDW superconductors. During the cooling process, S continuously increases from negative values, approaches zero, becomes positive, and then increases further. An anomaly occurs at the CDW transition tempera-

ture, T_{CDW}. In 4H-$NbSe_2$, this temperature corresponds to the maximum slope of the S–T curve, where the rate of increase in S diminishes below T_{CDW}. In contrast, for 2H-$NbSe_2$, the anomaly corresponds to the minimum slope, and below T_{CDW}, S no longer increases but instead decreases. In summary, the S–T behavior of La_3Al bears a higher resemblance to that of 4H-$NbSe_2$ than to 2H-$NbSe_2$. However, whether the transition occurring in La_3Al around 40–50 K is definitively a CDW transition remains an open question, necessitating further experimental investigation.

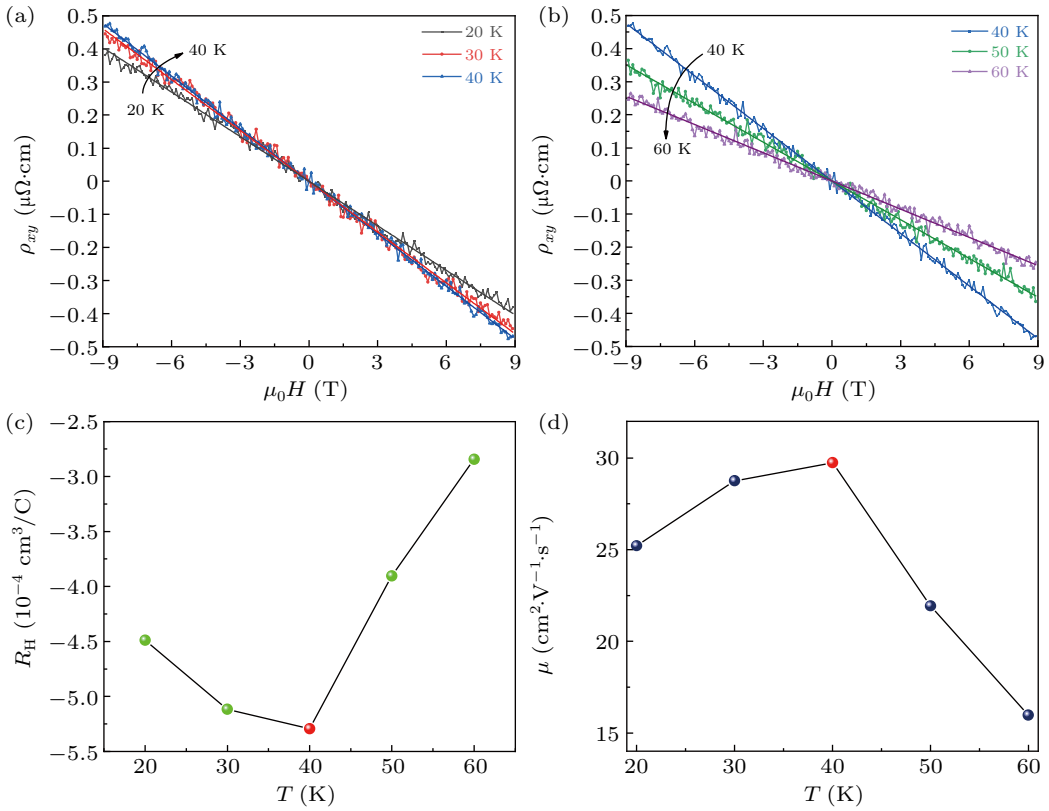


Fig. 3. Magnetic field and temperature dependence of Hall effect in La_3Al. (a) and (b) Field dependence of the Hall resistivity $\rho_{xy}(T, \mu_0 H)$ at several typical temperatures. (c) Temperature dependence of Hall coefficient. (d) Temperature dependence of carrier mobility.

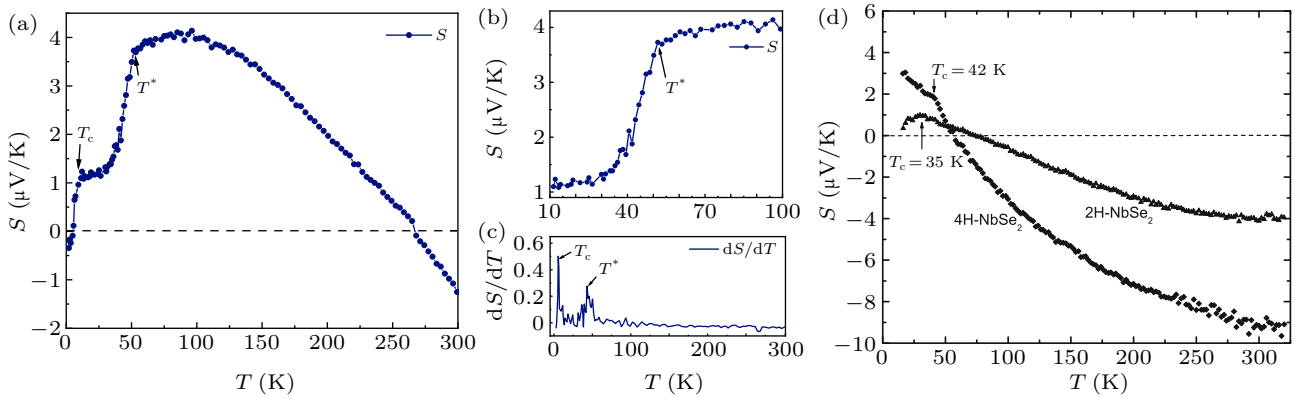


Fig. 4. The thermoelectric properties of La_3Al. (a) S–T curve from 2 K to 300 K. (b) The enlarged S–T curve from 10 K to 100 K. (c) The $\mathrm{d}S/\mathrm{d}T$–T curve from 2 K to 300 K. (d) S–T curve of 4H-$NbSe_2$ and 2H-$NbSe_2$ from Ref. [52].

Figure 5(a) depicts the reduction in critical temperature (T_c) as the external magnetic field increases from 0 T to 5 T. We employed the mid-transition temperature T_c^{mid} and presented a summary in Fig. 5(b). The $\mu_0 H_{c2}(T)$ curve exhibits a slight upward curvature near T_c, which cannot be fitted well using the GL formula. We observed that in the S–T curve spanning 2–300 K, S transitions from negative to positive and subsequently reverts to negative as the temperature decreases to 2 K. This behavior indicates that the dominant charge carrier type within La_3Al varies across different temperature ranges. Moreover, as revealed by subsequent density functional theory (DFT) calculations and shown below in Fig. 7(a), the band structure near the Fermi surface exhibits the coexistence of both hole and electron pockets. Collectively, these findings

suggest that La_3Al is a potential multi-band superconductor. Therefore, we fitted its upper critical field using the following two-band model:[53]

$$a_0\left[\ln t+U(h)\right]\left[\ln t+U(\eta h)\right]+a_2\left[\ln t+U(\eta h)\right]+a_1\left[\ln t+U(h)\right]=0, \tag{1}$$

where

$$t=T/T_c,\ \ U(x)=\psi\left(x+\frac{1}{2}\right)-\psi\left(\frac{1}{2}\right),\ \ \eta=\frac{D_2}{D_1},$$
$$h=\frac{\hbar\mu_0 H_{c2}D_1}{2\Phi_0 k_B T},\ \ a_0=\frac{2\omega}{\lambda_0},\ \ a_1=1+\frac{\lambda_-}{\lambda_0},$$
$$a_2=1-\frac{\lambda_-}{\lambda_0},\ \ \omega=\lambda_{11}\lambda_{22}-\lambda_{12}\lambda_{21},\ \ \lambda_-=\lambda_{11}-\lambda_{22},$$
$$\lambda_0=\sqrt{\lambda_-^2-4\lambda_{12}\lambda_{21}}.$$

Here $\psi(x)$ is a digamma function, D_1 and D_2 are intraband diffusivities of band 1 and band 2, ω, λ_- and λ_0 depend on intraband coupling strengthes λ_{11}, λ_{22} and interband coupling strengthes λ_{12}, λ_{21}. The data were well fitted with the two-band model. The red line gives a two-band fit of the data in the whole region, which indicates the possible multiband superconductivity in La_3Al compound. The estimated value of $\mu_0 H_{c2}(0)$ is 6.69 T.

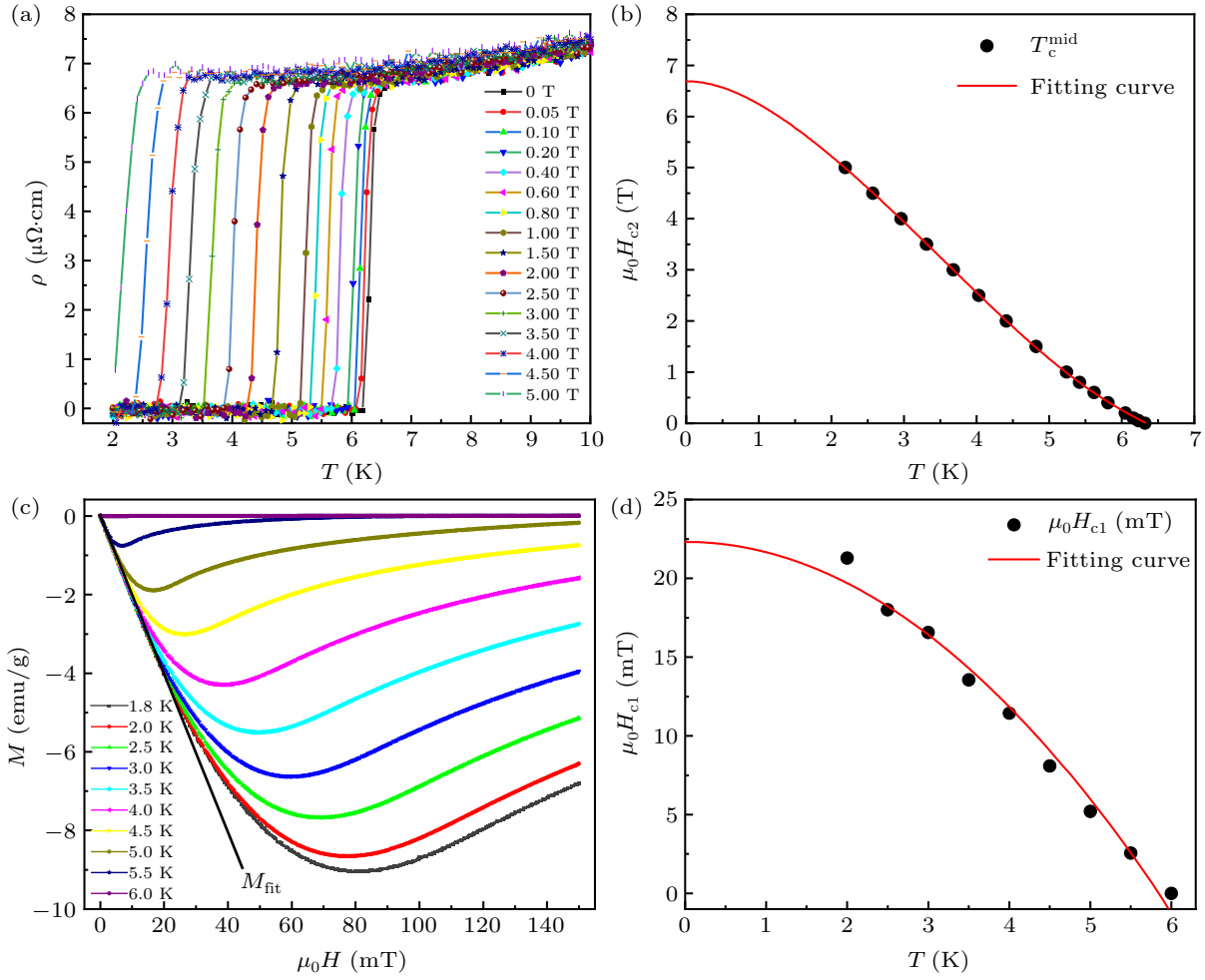


Fig. 5. (a) Temperature dependence of the resistivity at various external fields. (b) Transition temperatures extracted from (a) and the respective fitting using the two-band model. (c) Magnetic hysteresis of La_3Al at various temperatures. (d) Lower critical field $\mu_0 H_{c1}$ of La_3Al as a function of temperature. The red line is a linear fit.

The Pauli–Clogston field is

$$\mu_0 H_p(0)=1.84T_c^{zero}=11.37\ \text{T}, \tag{2}$$

which is much larger than the field we obtain from the empirical formula. The coherence length (ξ) can be acquired from the Ginzburg–Landau (GL) equation

$$\mu_0 H_{c2}(0)=\frac{\Phi_0}{2\pi\xi^2}, \tag{3}$$

where $\Phi_0=2.07\times10^{-15}$ T·m^2 is the magnetic flux unit. Using $\mu_0 H_{c2}(0)=6.69$ T, the calculated ξ is 7.01 nm. The magnetization versus external field over a range of temperatures below T_c is presented in Fig. 5(c). The deviation of the field from a linear curve representing the full Meissner effect was identified as the lower critical field at each temperature and is

presented in Fig. 5(d). Using the Ginzburg–Landau equation

$$\mu_0 H_{c1} = \mu_0 H_{c1}(0)\left(1-\left(\frac{T}{T_c}\right)^2\right), \tag{4}$$

we obtain a well-fitted curve, which yields $\mu_0 H_{c1}(0) = 22.17$ mT. Using the formula

$$\mu_0 H_{c1}(0) = \frac{\Phi_0}{4\pi\lambda^2}\ln\left(\frac{\lambda}{\xi}\right), \tag{5}$$

we obtain the penetration depth $\lambda = 151.04$ nm. The calculated GL parameter of $\kappa = (\lambda/\xi) \sim 21.55$ confirms the type-II superconductivity in La_3Al.

Figure 6 illustrates the analysis of the superconducting transition via heat-capacity measurements. The distinct anomaly observed at 6.07 K indicates the presence of bulk superconductivity. We fitted the normal-state heat capacity according to the following equation:

$$\frac{C_p(T)}{T} = \gamma + \beta T^2. \tag{6}$$

The extrapolation gives $\gamma = 13.1301$ mJ/(mol·K^2) and $\beta = 2.4983$ mJ/(mol·K^4), where γ is the Sommerfeld electronic specific heat coefficient and β is the phonon specific heat coefficient. Using the formula

$$\beta = N\frac{12\pi^4}{5\Theta_D^3}R, \tag{7}$$

and $N = 4$ for La_3Al, we obtain a Debye temperature of $\Theta_D = 146$ K. The electronic contribution $C_e(T)$ is obtained by subtracting the phononic contributions from C_p as presented in the inset of Fig. 6. The normalized jump in $C_e(T)$ is calculated to be $\Delta C_e/(\gamma T_c) = 2.16$, which is larger than that of the BCS anticipated value of 1.43, indicating an enhanced electron–phonon coupling in La_3Al.

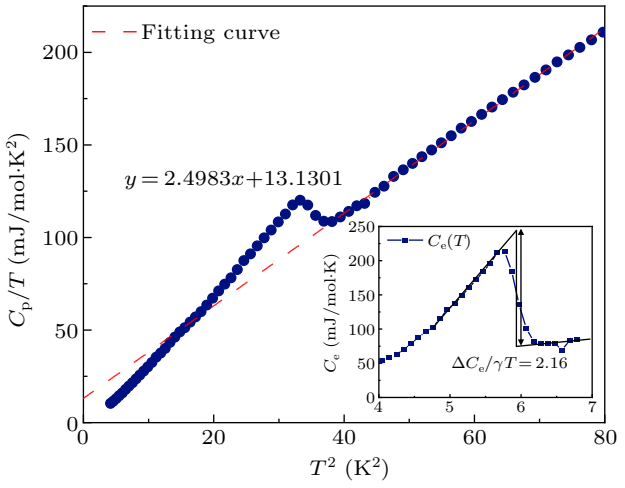


Fig. 6. Specific heat capacity of La_3Al from 4.0 K^2 to 80 K^2. Inset is the electronic specific heat capacity from 4.0 K to 6.8 K.

We further estimate the electron–phonon coupling constant λ_{ep} using the McMillan relation[54]

$$\lambda_{ep} = \frac{1.04 + \mu^* \ln\left(\frac{\Theta_D}{1.45T_c}\right)}{(1-0.62\mu^*)\ln\left(\frac{\Theta_D}{1.45T_c}\right) - 1.04}, \tag{8}$$

where μ^* is the Coulomb screening parameter (here, we set it at 0.13), and we take $T_c = T_c^{zero}$. $\lambda_{ep} = 0.92$ is thus obtained, indicating that La_3Al hosts an intermediately coupling strength. Moreover, the DOS at Fermi level (E_F) is estimated using the following equation:

$$N(E_F) = \frac{3\gamma}{\pi^2 k_B^2 (1+\lambda_{ep})}, \tag{9}$$

based on γ and λ_{ep}, yielding $N(E_F) = 2.9010$ eV^{-1}·f.u.$^{-1}$. Table 1 summarizes the superconducting parameters of La_3Al.

Table 1. Superconducting and thermodynamic parameters of La_3Al.

Parameter	Units	La_3Al
T_c^{zero}	K	6.18
$\mu_0 H_{c1}(0)$	mT	22.17
$\mu_0 H_{c2}(0)$	T	6.69
ξ_{GL}	nm	7.01
λ_{GL}	nm	151.04
κ_{GL}		21.55
γ	mJ/(mol·K^2)	13.1301
Θ_D	K	146
λ_{ep}		0.92
$\Delta C_{es}/(\gamma T_c)$		2.16
$N(E_F)$	states·eV^{-1}·f.u.$^{-1}$	2.9010

3.3. First-principles calculations

To gain deeper insight into the characteristics of La_3Al, we conducted density functional theory (DFT) calculations to analyze its electronic band structures. The band structures of La_3Al in the vicinity of the Fermi level (E_F) are depicted in Fig. 7(a). The dashed lines represent the results obtained without considering spin–orbit coupling (SOC), while the red solid lines illustrate the results incorporating SOC effects. Regardless of SOC effects, we find that there are multiple energy bands crossing the Fermi surface, which is consistent with the good metallic properties shown in the La_3Al electrical transport curve. It is noteworthy that the inclusion of SOC did lead to notable alterations in the band dispersion near the Fermi level through band splitting (regions 2 and 4 of Fig. 7(a)) or change from two intersecting bands to new energy bands (regions 1 and 3 of Fig. 7(a)). Figures 7(b) and 7(c) illustrate the calculated total density of states (DOS) for La_3Al. The DOS near the Fermi energy in La_3Al primarily originates from the La states, with Al states making relatively minor contributions. Considering that the energy bands from La dominate the DOS of La_3Al around Fermi energy, the superconducting states in La_3Al are predominantly attributed to the states of La atom forming the kagome lattice.

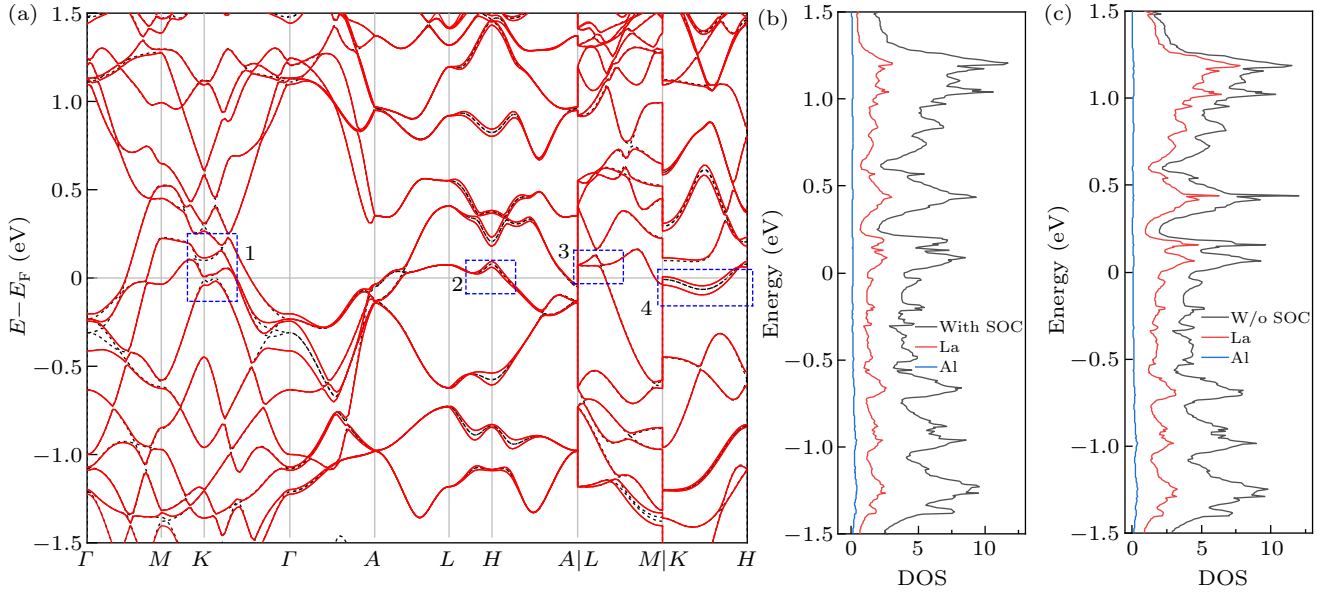


Fig. 7. (a) Calculated electronic band structure of La_3Al without and with SOC near the Fermi level. The corresponding DOS plots are shown in (b) and (c), respectively.

4. Conclusion

In this work, we synthesize La_3Al and analyze the superconducting properties of La_3Al, which is a La-based kagome superconductor. The compound exhibits a sharp superconducting transition at $T_c^{onset} = 6.37$ K and $T_c^{zero} = 6.18$ K, with lower and upper critical fields of 22.17 mT and 6.69 T, respectively. Hall resistivity data revealed a significant upturn behavior below the resistivity anomaly, in analogue to the observations in AV_3Sb_5 (A = K, Rb, Cs) that intertwined with CDW order. The measured heat capacity confirms the presence of bulk superconductivity, with a normalized specific heat change of $\Delta C_e/(\gamma T_c) = 2.16$ and an electron–phonon strength of $\lambda_{ep} = 0.92$. Further analysis reveals that La_3Al is an intermediately coupled type-II BCS superconductor. Such study will deepen our understanding of superconducting materials with kagome lattice.

Acknowledgments

Project supported by the National Natural Science Foundation of China (Grant Nos. 52272268 and 52250308), the Strategic Priority Research Program and Key Research Program of Frontier Sciences of the Chinese Academy of Sciences (Grant No. XDB33010100), the Informatization Plan of Chinese Academy of Sciences (Grant No. CAS-WX2021SF-0102), and the Synergetic Extreme Condition User Facility (SECUF).

References

[1] Yin J X, Lian B and Hasan M Z 2022 *Nature* **612** 647
[2] Chowdhury N, Khan K I A, Bangar H, Gupta P, Yadav R S, Agarwal R, Kumar A and Muduli P K 2023 *Proceedings of the National Academy of Sciences, India Section A: Physical Sciences* **93** 477
[3] Han T H, Helton J S, Chu S, Nocera D G, Rodriguez-Rivera J A, Broholm C and Lee Y S 2012 *Nature* **492** 406
[4] Yan S, Huse D A and White S R 2011 *Science* **332** 1173
[5] Balents L 2010 *Nature* **464** 199
[6] Olariu A, Mendels P, Bert F, Duc F, Trombe J C, De Vries M A and Harrison A 2008 *Phys. Rev. Lett.* **100** 087202
[7] Xue H, Yang Y, Gao F, Chong Y and Zhang B 2019 *Nat. Mater.* **18** 108
[8] Liu E, Sun Y, Kumar N, Muechler L, Sun A, Jiao L and Felser C 2018 *Nat. Phys.* **14** 1125
[9] Ye L, Kang M, Liu J, Von Cube F, Wicker C R, Suzuki T and Checkelsky J G 2018 *Nature* **555** 638
[10] Peng C, Jiang Y F, Sheng D N and Jiang H C 2021 *Adv. Quantum Technol.* **4** 2000126
[11] Wang Q, Qiu X L, Pei C, Gong B C, Gao L, Zhao Y and Qi Y 2023 *New J. Phys.* **25** 043001
[12] Jiang K, Wu T, Yin J X, Wang Z, Hasan M Z, Wilson S D and Hu J 2023 *Natl. Sci. Rev.* **10** nwac199
[13] Chen H, Hu B, Ye Y, Yang H and Gao H J 2022 *Chin. Phys. B* **31** 097405
[14] Ortiz B R, Sarte P M, Kenney E M, Graf M J, Teicher S M, Seshadri R and Wilson S D 2021 *Phys. Rev. Mater.* **5** 034801
[15] Ortiz B R, Teicher S M L, Hu Y, Zuo J L, Sarte P M, Schueller E C, Abeykoon A M M, Krogstad M J, Rosenkranz S, Osborn R, Seshadri R, Balents L, He J and Wilson S D 2020 *Phys. Rev. Lett.* **125** 247002
[16] Ni S, Ma S, Zhang Y, *et al*. 2021 *Chin. Phys. Lett.* **38** 057403
[17] Mielke III C, Das D, Yin J X, Liu H, Gupta R, Jiang Y X, Medarde M, Wu X, Lei H C, Chang J, Dai P, Si Q, Miao H, Thomale R, Neupert T, Shi Y, Khasanov R, Hasan M Z, Luetkens H and Guguchia Z 2022 *Nature* **602** 245
[18] Luo H, Gao Q, Liu H, Gu Y, Wu D, Yi C, Jia J, Wu S, Luo X, Xu Y, Zhao L, Wang Q, Mao H, Liu G, Zhu Z, Shi Y, Jiang K, Hu J, Xu Z and Zhou X J 2022 *Nat. Commun.* **13** 273
[19] Chen H, Yang H, Hu B, *et al*. 2021 *Nature* **599** 222
[20] Cho S, Ma H, Xia W, Yang Y, Liu Z, Huang Z, Jiang Z, Lu X, Liu J, Liu Z, Li J, Wang J, Liu Y, Jia J, Guo Y, Liu J and Shen D 2021 *Phys. Rev. Lett.* **127** 236401
[21] Chen K Y, Wang N N, Yin Q W, Gu Y H, Jiang K, Tu Z J, Gong C S, Uwatoko Y, Sun J P, Lei H C, Hu J P and Cheng J G 2021 *Phys. Rev. Lett.* **126** 247001
[22] Chen X, Zhan X, Wang X, Deng J, Liu X B, Guo J G and Chen X 2021 *Chin. Phys. Lett.* **38** 057402
[23] Song Y, Ying T, Chen X, Han X, Wu X, Schnyder A P, Huang Y, Guo J G and Chen X 2021 *Phys. Rev. Lett.* **127** 237001
[24] Yang Y, Wang R, Shi M Z, Wang Z, Xiang Z and Chen X H 2021 *Phys. Rev. B* **104** 245128
[25] Yang Y, Fan W, Zhang Q, Chen Z, Chen X, Ying T, Wu X, Yang X, Meng F, Li G and Li S 2021 *Chin. Phys. Lett.* **38** 127102

[26] Yin Q, Tu Z, Gong C, Tian S and Lei H 2021 *Chin. Phys. Lett.* **38** 127401
[27] Po H C, Vishwanath A and Watanabe H 2017 *Nat. Commun.* **8** 50
[28] Chen Y Y, Lawrence J M, Thompson J D and Willis J O 1989 *Phys. Rev. B* **40** 10766
[29] Medina A, Hayashi M, Cardoso L, *et al*. 1998 *Phys. Rev. B* **57** 5900
[30] Chen Y Y, Yao Y D, Hu B C, Jang C H, Lawrence J M, Huang H and Li W H 1997 *Phys. Rev. B* **55** 5937
[31] Li L, Yamagata R, Nishimura K and Yamaoka H 2009 *Phys. Rev. B* **80** 134429
[32] Singh D, Yadam S, Venkateshwarlu D, Gangrade M, Samatham S S and Ganesan V 2014 *Mater. Res. Express* **1** 046114
[33] Huang L and Lu H 2020 *Phys. Rev. B* **102** 155140
[34] Singh D, Patidar M M, Ganesan V and Suresh K G 2020 *J. Magn. Magn. Mater.* **514** 167184
[35] Fukuhara T, Yamagata R, Li L, Nishimura K and Maezawa K 2009 *J. Phys. Soc. Jpn.* **78** 034723
[36] Singh D, Nag J, Yadam S, Ganesan V, Alam A and Suresh K G 2023 *Appl. Phys. Lett.* **123** 171902
[37] Sakurai T, Marushita Y, Fujiwara H, Kadomatsu H, Oguro I and Sakurai J 1992 *J. Magn. Magn. Mater.* **115** 250
[38] Smith T F and Luo H L 1967 *J. Phys. Chem. Solids* **28** 569
[39] Kuwasawa Y, Sekizawa K, Usui N and Yasukochi K 1969 *J. Phys. Soc. Jpn.* **27** 590
[40] Mamiya T, Aoi T, Iwahashi K and Masuda Y 1971 *J. Phys. Soc. Jpn.* **31** 485
[41] Aoi T and Masuda Y 1974 *J. Phys. Soc. Jpn.* **37** 673
[42] Aoi T and Masuda Y 1974 *Low Temperature Physics-LT* 13 Volume 2: Quantum Crystals and Magnetism (Boston, MA: Springer US) p. 574
[43] Momma K and Izumi F 2011 *J. Appl. Cryst.* **44** 1272
[44] Kresse G and Furthmüller J 1996 *Comput. Mater. Sci.* **6** 15
[45] Perdew J P, Burke K and Ernzerhof M 1996 *Phys. Rev. Lett.* **77** 3865
[46] Kresse G and Joubert D 1999 *Phys. Rev. B* **59** 1758
[47] Monkhorst H J and Pack J D 1976 *Phys. Rev. B* **13** 5188
[48] Yu F H, Wu T, Wang Z Y, Lei B, Zhuo W Z, Ying J J and Chen X H 2021 *Phys. Rev. B* **104** L041103
[49] Yang S Y, Wang Y, Ortiz B R, Liu D, Gayles J, Derunova E, Gonzalez-Hernandez R, Šmejkal L, Chen Y, Parkin S S P, Wilson S D, Toberer E S, McQueen T and Ali M N 2020 *Sci. Adv.* **6** eabb6003
[50] Yin Q, Tu Z, Gong C, Fu Y, Yan S and Lei H 2021 *Chin. Phys. Lett.* **38** 037403
[51] Naito M and Tanaka S 1982 *J. Phys. Soc. Jpn.* **51** 219
[52] Naik I and Rastogi A K 2011 *Pramana-J. Phys.* **76** 957
[53] Gurevich A 2003 *Phys. Rev. B.* **67** 184515
[54] McMillan W L 1968 *Phys. Rev.* **167** 331